

COUPLED EVOLUTION WITH TIDES OF THE RADIUS AND ORBIT OF TRANSITING GIANT PLANETS: GENERAL RESULTS

LAURENT IBGUI¹, ADAM BURROWS¹

¹Department of Astrophysical Sciences, Peyton Hall, Princeton University, Princeton, NJ 08544

Accepted for publication in ApJ, June 2, 2009

ABSTRACT

Some transiting extrasolar giant planets have measured radii larger than predicted by the standard theory. In this paper, we explore the possibility that an earlier episode of tidal heating can explain such radius anomalies and apply the formalism we develop to HD 209458b as an example. We find that for strong enough tides the planet’s radius can undergo a transient phase of inflation that temporarily interrupts canonical, monotonic shrinking due to radiative losses. Importantly, an earlier episode of tidal heating can result in a planet with an inflated radius, even though its orbit has nearly circularized. Moreover, we confirm that at late times, and under some circumstances, by raising tides on the star itself a planet can spiral into its host. We note that a 3× to 10×solar planet atmospheric opacity with no tidal heating is sufficient to explain the observed radius of HD 209458b. However, our model demonstrates that with an earlier phase of episodic tidal heating we can fit the observed radius of HD 209458b even with lower (solar) atmospheric opacities. This work demonstrates that, if a planet is left with an appreciable eccentricity after early inward migration and/or dynamical interaction, coupling radius and orbit evolution in a consistent fashion that includes tidal heating, stellar irradiation, and detailed model atmospheres might offer a generic solution to the inflated radius puzzle for transiting extrasolar giant planets such as WASP-12b, TrES-4, and WASP-6b.

Subject headings: planetary systems — planets and satellites: general

1. INTRODUCTION

The most useful experimental data constraining evolutionary models of extrasolar planets and their radii (R_p) come from measurements of transiting planets¹. The radius of a transiting planet is inferred from transit lightcurve measurements, which in combination with radial velocity measurements remove the planet mass M_p - inclination angle degeneracy. Much theoretical effort has been undertaken to model, and then to understand, the measured radii (Guillot et al. 1996; Burrows et al. 2000; Bodenheimer et al. 2001; Burrows et al. 2003; Bodenheimer et al. 2003; Baraffe et al. 2003; Burrows et al. 2004; Fortney & Hubbard 2004; Baraffe et al. 2004; Chabrier et al. 2004; Laughlin et al. 2005; Baraffe et al. 2005, 2006; Burrows et al. 2007; Fortney et al. 2007; Marley et al. 2007; Chabrier & Baraffe 2007; Liu et al. 2008; Baraffe et al. 2008).

As Burrows et al. (2007) have emphasized, custom fits are preferred for each planet to “project out” the effects of age, planet mass, stellar flux, etc. before one can conclude whether a measured transit radius can or cannot be reproduced by theory. Indeed, the transit radius of an extrasolar giant planet (EGP) depends on many parameters (see Burrows et al. 2007 for a sensitivity study). These include the planet mass, the stellar irradiation flux F_p , the transit radius effect (Burrows et al. 2003; Baraffe et al. 2003), the atmospheric composition, the presence of heavy elements in

the envelope or in a central core, atmospheric circulation that couples the day and the night sides, the planet’s age, and any effects that could generate an extra power source in the interior of the planet. It had once been thought such extra power could be due to obliquity tides when the planet is in a Cassini state (Winn & Holman 2005), but such a possibility has now largely been ruled out (Levrard et al. 2007; Fabrycky et al. 2007). However, heating due to the penetration and dissipation at depth of gravity waves (Guillot & Showman 2002; Showman & Guillot 2002), or strong tidal effects (Bodenheimer et al. 2003; Liu et al. 2008; Jackson et al. 2008b,c,d) have not been eliminated. The latter could be due the pumping of eccentricity by an undetected companion (Bodenheimer et al. 2001; Mardling 2007). We note that it is not known whether the tidal heat is deposited predominantly in the convective core (Ogilvie & Lin 2004; Goodman & Lackner 2008) or in the radiative envelope (Wu 2005a). We make the default assumption of all planet radius evolutionary modelers to date that it is deposited in the core, but the reader is encouraged to keep an open mind.

The initial conditions assumed for our simulations can affect the structures of EGPs at young ages (\lesssim a few 10 Myr). As a consequence, a model of planet formation would be useful to determine the planet’s initial entropy and, therefore, its early radius (Marley et al. 2007; Fortney et al. 2008). However, since the ages of the mature transiting EGPs discovered so far are a few Gyrs, precise initial entropies are not crucial for our study. On the other hand, as we show in this paper, if tidal effects in the planet or in the star are taken into account, the orbital parameters of eccentricity and semi-major axis left after formation, early evolution and migration (Goldreich & Sari 2003), planet-planet scattering

Electronic address: ibgui@astro.princeton.edu, burrows@astro.princeton.edu

¹ See J. Schneider’s Extrasolar Planet Encyclopaedia at <http://exoplanet.eu>, the Geneva Search Programme at <http://exoplanets.eu>, and the Carnegie/California compilation at <http://exoplanets.org>.

(Ford et al. 2003; Chatterjee et al. 2008; Ford & Rasio 2008; Jurić & Tremaine 2008), or the operation of the Kozai mechanism (Wu & Murray 2003; Wu 2003; Wu et al. 2007; Nagasawa et al. 2008) do matter.

There are two classes of discrepancies between measured transit radii and theoretical predictions. The first is the subset comprised of those EGPs larger than default radius predictions and includes HD 209458b (Charbonneau et al. 2000; Knutson et al. 2007), TrES-4 (Mandushev et al. 2007), WASP-12b (Hebb et al. 2009), WASP-4b (Wilson et al. 2008; Gillon et al. 2009b), WASP-6b (Gillon et al. 2009a), XO-3b (Johns-Krull et al. 2008; Winn et al. 2008), and HAT-P-1b (Bakos et al. 2007; Winn et al. 2007; Johnson et al. 2008). The other class consists of EGPs that are in fact smaller than default predictions without dense cores and, therefore, seem to require such cores (Guillot et al. 2006; Burrows et al. 2007). The correlation Guillot et al. (2006) and Burrows et al. (2007) discovered between the inferred core mass and the stellar metallicity, which is not used in the modeling, supports both the notion that dense cores are present and the core accretion mechanism for giant planet formation.

Previously, Burrows et al. (2007) studied the effects of an extra heat source (\dot{E}_{tide}) in the planet’s interior and estimated the power necessary to explain some of the measured radii. Liu et al. (2008) took this a step further by incorporating core tidal heating to explain the observed radii of TrES-4, XO-3b, and HAT-P-1b, but kept their orbital parameters constant at currently observed values. Jackson et al. (2008b,c,d) studied the coupled evolution of e , a and \dot{E}_{tide} of close-in EGPs, but maintained a constant planetary radius.

However, and importantly, Jackson et al. (2008b,c,d) and Gu et al. (2003) highlighted the possible role of tidal orbital evolution in inflating the radius of an exoplanet. In this paper, we verify their original insight by consistently and simultaneously coupling the evolution of R_p , e , a , \dot{E}_{tide} , and F_p ($\dot{E}_{\text{insolation}}$) in the context of a sophisticated atmosphere and irradiation model for the planet. We take into account the tides raised on the planet and the tides raised on the star. We find that if the tides are strong enough a planet’s radius can undergo a transient phase of inflation that temporarily interrupts shrinking, and does so at epochs consistent with the few Gyr ages of transiting planets. Extremely strong tides fade at a very early stage and have a negligible impact on the radius at Gyr ages. It is noteworthy that the behavior is nonlinear and depends sensitively on the initial orbital conditions and on tidal heating parameters. In addition, we find that increasing the planet’s atmospheric opacity accelerates and increases the magnitude of the transient effect. If the tides raised on the star are negligible, the orbit reaches a final circular equilibrium state. Otherwise, there is no final equilibrium, and the planet might eventually plunge into its host star (Rasio et al. 1996; Levrard et al. 2009). We find that due to an earlier phase of tidal heating a planet whose orbit has circularized can still have an inflated radius. As an example and proof of principle, we apply our formalism to HD 209458b. We find a set of tidal parameters, Q'_p and Q'_* , and initial orbital parameters, e_i and a_i , that lead to the measured values of R_p , a , e , even for atmospheric opacities for so-

lar equilibrium abundances. We find that HD 209458b’s radius can also be fit with no tides and a $3\times$ to $10\times$ solar planet atmospheric opacity at the new and shorter age of ~ 3.1 Gyrs suggested by Torres et al. (2008). However, unless the atmospheric abundances can be measured, it will be difficult to distinguish the different predictions, particularly given the current ambiguity in Q' . Nevertheless, if there are independent (theoretical?) constraints on Q' , and/or precision measurements of the atmospheric spectra, one might be able to discriminate between the two different explanations.

In §2, we present our formalism, model assumptions, and computational techniques. Section 3 is the central section of the paper in which we describe the generic coupled evolution of R_p , e , a , $\dot{E}_{\text{tide}}/\dot{E}_{\text{insolation}}$ when tides play a significant role. We describe in §3.1 the typical scenario, which exhibits transient radius inflation due to tidal heating of the planet. The case of extremely strong tides is discussed in §3.2. In §3.3, we address the effect of atmospheric opacity and in §3.4 we analyze the influence of the tides raised on the star. The latter can cause the planet to spiral in. In §4, we apply the model to HD 209458b. Finally, in §5 we summarize our results, review caveats, and discuss how such transient tidal heating might explain other large-radius EGPs, such as WASP-12b, TrES-4, and WASP-6b.

2. MODEL: FORMALISM, ASSUMPTIONS, AND COMPUTATIONAL TECHNIQUES

The evolution of a planet’s eccentricity and semi-major axis due to tidal effects depends sensitively on its radius. In turn, the evolution of its radius depends sensitively on the tidal heating power in its interior associated with the corresponding evolution of its orbital parameters. Moreover, a planet’s radius evolution is sensitive to the degree of stellar irradiation, which is directly tied to the planet-star distance. Therefore, to perform simultaneous orbital and radius evolutions, all the relevant equations must be coupled and atmospheric boundary conditions that vary systematically with changing irradiation regimes must be incorporated. We have established the tools necessary to self-consistently accomplish such calculations and in this section we describe our methods.

We assume that the planet has a spherical gaseous H_2 , He envelope, and use the equation of state of Saumon et al. (1995). The helium mass fraction (Y) is set equal to 0.25. The effect of reasonable variations in Y on the radius of an EGP is small. Except in the atmosphere, we assume the planet is fully convective and that its envelope contains no heavy elements. Though our formalism allows it, in this paper we ignore the possible effects of an inner dense core. As shown, for instance, in Guillot et al. (2006) and Burrows et al. (2007), the presence of heavy elements in either the envelope or the core decreases the total radius of the EGP. To model the evolution of the planet, we use the Henyey evolutionary code of Burrows et al. (1993, 1997), with boundary conditions that incorporate realistic irradiated planetary atmospheres. Using COOLTLUSTY, a variant of the spectral atmosphere code TLUSTY (Hubeny & Lanz 1995), we precalculate grids of atmospheres for various values of T_{eff} and surface gravity g . These provide the associated entropy S in the convective region of the planet. Inverting the relation to obtain $T_{\text{eff}}(S, g)$ yields the energy flux

escaping the interior (“ σT_{eff}^4 ”; Burrows et al. 2003). We precalculate these grids not only for a given gravity and T_{eff} , but also for each orbital pair (e, a). The stellar flux at the planet is taken to be the time-averaged mean during an orbit. Thus, we have atmospheric and evolutionary boundary conditions which follow the evolution of the planetary orbit. The stellar spectrum is interpolated at the actual effective temperature and gravity of the star from the Kurucz stellar atmosphere models (Kurucz 1994). Note that we assume the stellar spectrum is constant during evolution. We include the “transit radius effect,” which accounts for the fact that the transit radius is an impact parameter (Burrows et al. 2003; Baraffe et al. 2003).

In our calculations, we assume that tidal heating occurs entirely in the convective interior of the planet and that the evolutionary process starts a few Myr after the star’s formation. Therefore, we suppose that the protoplanetary disk has dissipated (Goldreich & Sari 2003) and that any ensuing chaotic collisional period of planet-planet scattering has ended (Ford et al. 2003; Jurić & Tremaine 2008; Chatterjee et al. 2008; Ford & Rasio 2008; Nagasawa et al. 2008). Importantly, we presume that, after these early formation, migration, and dynamical phases, an interesting subset of close-in EGPs are left with high values of e_i ($\gtrsim 0.2$) and small values of the “initial” semi-major axes, a_i ($\lesssim 0.1 - 0.15$ AU). (a_i is still larger than the “final” values currently observed.) These assumptions are necessary for tidal effects to be of interest as a possible explanation for the large planetary radii observed in a subset of cases and are not unreasonable (Ford & Rasio 2008; Nagasawa et al. 2008). We neglect stellar and planetary obliquities, assume that the planet’s spin is synchronized (is tidally locked) with its orbital period, and that the star’s spin rate is small compared with the orbital mean motion. A rough estimate of the synchronization time (τ_{sync}) for a close-in EGP gives a value between one and a few $\times 10$ Myr (Guillot et al. 1996). We assume that equilibrium tides have a constant lag angle for any frequency and that Q' is independent of orbital period. Another approach is to assume a constant time lag for any frequency, as was done in the pioneering work of Darwin (1880) (see also Hut 1981, Rasio et al. 1996, Eggleton et al. 1998, and Levrard et al. 2009). Higher-order e formulations, though developed (Mardling & Lin 2002; Ogilvie & Lin 2004; Dobbs-Dixon et al. 2004; Mardling 2007), introduce numerous other uncertain approximations concerning tidal processes. Given our current limited knowledge of tidal dissipation/heating in EGPs, we feel the approach we have employed is acceptable.

With all these assumptions, the equations of tidal evolution of eccentricity e , semi-major axis a , and tidal heating rate \dot{E}_{tide} , to second order in eccentricity, are (Goldreich & Soter 1966; Kaula 1968; Peale & Cassen 1978; Murray & Dermott 1999; Bodenheimer et al. 2001, 2003; Gu et al. 2004; Mardling 2007; Jackson et al.

2008c,d,a; Ferraz-Mello et al. 2008; Barnes et al. 2009):

$$\frac{1}{e} \frac{de}{dt} = -\frac{1}{a^{13/2}} \left[\overbrace{K_{1p*} \frac{R_p^5}{Q_p'}} + \overbrace{K_{2p*} \frac{R_*^5}{Q_*'}} \right], \quad (1)$$

$$\frac{1}{a} \frac{da}{dt} = -\frac{1}{a^{13/2}} \left[\underbrace{2K_{1p*} \frac{R_p^5}{Q_p'} e^2}_{\text{tides on planet}} + \underbrace{\frac{8}{25} \left(1 + \frac{57}{4} e^2\right) K_{2p*} \frac{R_*^5}{Q_*'}}_{\text{tides on star}} \right], \quad (2)$$

and

$$\dot{E}_{\text{tide}} = \left(\frac{63}{4} G^{3/2} M_*^{5/2} \right) \frac{R_p^5}{Q_p'} \frac{e^2}{a^{15/2}}, \quad (3)$$

where K_{1p*} and K_{2p*} are constants defined by

$$K_{1p*} = \frac{63}{4} G^{1/2} \frac{M_*^{3/2}}{M_p} \quad (4)$$

$$K_{2p*} = \frac{225}{16} G^{1/2} \frac{M_p}{M_*^{1/2}}, \quad (5)$$

G is the gravitational constant, and M_p , M_* , R_p , R_* are the masses and radii of the planet and star. Note that the planet radius is time-dependent ($R_p(t)$), but the star’s radius is assumed to be constant. The evolution of e and a are due both to tides raised on the planet (due to the star) and tides raised on the star (due to the planet). Equations (1) and (2) indicate that e and a can only decrease. This is because we assume the stellar spin rate is low. This is different from, for example, the Earth-Moon system, for which the tides raised on the Earth increase the semi-major axis, while the tides raised on the Moon decrease it (Goldreich & Soter 1966). As Mardling (2007) has pointed out, eqs. (1), (2), and (3) don’t include the higher-order terms beyond e^2 and these terms should be important for high e . However, in this paper we focus on the generic character of the planet-orbit coupling and its potential role in explaining the subset of EGPs with anomalous radii. In this light, and given the many remaining ambiguities in tidal heating theory, our formalism should be adequate to address the central phenomena.

The Q' s in eqs. (1), (2), and (3) are the tidal dissipation factors (Q'_p in the planet and Q'_* in the star), given by $Q' = 3Q/2k_2$, where Q is the specific tidal dissipation function (Goldreich 1963) and k_2 is the Love number (Love 1927; Goldreich & Soter 1966; Ogilvie & Lin 2007). Smaller Q' s result in higher rates of tidal dissipation. For Jupiter, we have $Q' \approx 4Q$ (Gavrilov & Zharkov 1977) and estimates of Q are $\sim 6 \times 10^4 - 10^6$ (Goldreich & Soter 1966; Yoder & Peale 1981). Ogilvie & Lin (2004) have provided a theoretical motivation for values of Q near $\sim 10^5$. For a synchronized short-period EGP, we have only crude estimates, but Ogilvie & Lin (2004) propose values of $\sim 5 \times 10^6 - 10^7$ and Jackson et al. (2008b,c) propose values of $Q'_* \sim 10^{5.5}$

and $Q'_p \sim 10^{6.5}$. The latter are based on the statistical distribution of initial values of e and a the authors obtain after integrating eqs. (1) and (2) backwards in time at constant R_p . For terrestrial planets, the physics of tidal dissipation is different and it is thought that $Q' \gtrsim 10^2$ (Dickey et al. 1994; Mardling & Lin 2004; Jackson et al. 2008a). Most of the numerical values for this factor are empirically determined. For Jovian planets and EGPs there are various ongoing efforts to improve our understanding of tidal dissipation (Ogilvie & Lin 2004; Wu 2005a,b; Goodman & Lackner 2008), but there is as yet no comprehensive theory. Moreover, theory has yet to determine where in the planet the tidal heat is deposited. If it is not deposited in the convective core, but in the radiative atmosphere, our results might need to be altered. Goodman & Lackner (2008) have studied dynamical tides in an isentropic fluid body, focusing on inertial waves excited by scattering from the rigid core of a planet, and conclude that these waves might dissipate most of their energy in the convective region. This is also the suggestion of Ogilvie & Lin (2004). Wu (2005a), on the other hand, suggests that a large fraction of the tidal heat could be deposited in the outer regions, perhaps in the radiative zone. However, all modelers who have explored the possible effects of tidal heating on EGP radius evolution have assumed that the heat is deposited in the convective interior where it can be redistributed almost instantly. For specificity, we stick to this convention for this study, assume that Q' is a property of each body, and assume it is constant during the integration.

Since radius evolution must account for stellar irradiation, an informative quantity is the ratio between the tidal heating rate \dot{E}_{tide} and the insolation rate, $\dot{E}_{\text{insolation}} = \pi R_p^2 F_p$, where F_p is the flux at the substellar point. To second order in the eccentricity, this ratio is:

$$\frac{\dot{E}_{\text{tide}}}{\dot{E}_{\text{insolation}}} = \left(\frac{63}{4\pi\sigma} G^{3/2} \right) \left(\frac{M_*^{5/2}}{R_*^2 T_*^4} \right) \frac{R_p^3}{Q'_p} \frac{e^2}{a^{11/2}}, \quad (6)$$

where σ is the Stefan-Boltzmann constant and T_* is the effective temperature of the star. As is clear from eq. (6), this ratio is a very stiff function of a , and a moderately stiff function of R_p . We integrate forward in time equations (1) and (2), along with the Henyey equations of planetary structure and radius evolution which incorporate tidal heating given by eq. (3). We start at various arbitrarily specified initial eccentricities e_i and semi-major axes a_i and also specify Q'_p and Q'_* , keeping them constant during an integration. The strong non-linear coupling between e and a , already emphasized by Jackson et al. (2008c), is made all the more so in our more general formalism by the variation in R_p and the stiff dependence on R_p in eqs. (1) and (2).

From eqs. (1) and (2), we can estimate the relative contributions of the tides raised on the planet (due to the star) $[(de/dt)_P, (da/dt)_P]$ and raised on the star (due to

the planet) $[(de/dt)_*, (da/dt)_*]$. We obtain:

$$\frac{(de/dt)_P}{(de/dt)_*} = \frac{28}{25} \left(\frac{M_*}{M_P} \right)^2 \left(\frac{R_P}{R_*} \right)^5 \left(\frac{Q'_*}{Q'_P} \right), \quad (7)$$

$$\frac{(da/dt)_P}{(da/dt)_*} = \left(\frac{7e^2}{1 + \frac{57}{4}e^2} \right) \left(\frac{M_*}{M_P} \right)^2 \left(\frac{R_P}{R_*} \right)^5 \left(\frac{Q'_*}{Q'_P} \right). \quad (8)$$

The factor $[7e^2/(1 + 57e^2/4)]$ in eq. (8) ranges from $\simeq 0.46$ ($e = 1$) to zero ($e = 0$). If we assume that the EGP has the mass and the radius of Jupiter and orbits a sun-like host star, then the ratio given by eq. (7) is $(\dot{e}_P/\dot{e}_*) \simeq 14 (Q'_*/Q'_P)$ and the ratio given by eq. (8) is $(\dot{a}_P/\dot{a}_*) \simeq 88 (Q'_*/Q'_P) [e^2/(1 + 57e^2/4)]$. For HD 209458b, the factors 14 and 88 become 73 and 457, respectively. Thus, if the star is as dissipative as the planet ($Q'_* \sim Q'_P$) or less dissipative ($Q'_* > Q'_P$), then the evolution of the eccentricity is due mainly to the effect of the tides raised on the planet. However, if the dissipation inside the star is high enough ($Q'_* \ll Q'_P$), then the effect of the tides raised on the star has a comparable or even greater influence. Moreover, once the orbit is circular ($e = 0$), the tidal effect on the planet ceases (eq. 3), but since the planet and star are not synchronized the tidal effect on the star does not. As a consequence, the planet's orbital decay continues, though on a different timescale and it can eventually inspiral into its host star. Incidentally, when $e = 0$, eq. (2) can be integrated analytically to yield:

$$a = a_0 \left[1 - \frac{117}{4} \frac{G^{1/2}}{a_0^{13/2}} \frac{M_P}{M_*^{1/2}} \frac{R_*^5}{Q'_*} (t - t_0) \right]^{2/13}, \quad (9)$$

where a_0 is the semi-major axis at any time t_0 after the orbit has circularized. A similar formula is given in Goldreich (1963). This formula demonstrates that spiral in accelerates when the star is more dissipative (Q'_* lower), has a bigger radius R_* , has a lower mass M_* , or if the planet has a higher mass M_P .

3. THE GENERIC COUPLED EVOLUTION OF THE PLANETARY RADIUS, THE ECCENTRICITY, AND THE SEMI-MAJOR AXIS

In this section, we present and analyze the generic results of interest that have emerged from our calculations of the simultaneous evolution of the radius and orbital parameters of transiting (close-in) EGPs when tidal effects are included. The models assume various values of Q'_p and Q'_* , as well as representative initial values of the orbital parameters e_i and a_i , and are chosen to highlight various possible behaviors that might be germane to the explanation of the anomalous radii of a subset of the measured transiting EGPs. Moreover, for discussions of a “generic transiting system” we have employed the properties of HD 209458 and HD 209458b (listed in Table 1). However, it is important to point out that the values of the relevant parameters are specific to each individual planet-host star system. In each of the following subsections, we illustrate our conclusions with a four-panel figure (Figs. 1, 2, 3, and 4) in two rows, with $R_p(t)$ and

$e(t)$ on the first row, and $a(t)$ and $(\dot{E}_{\text{tide}}/\dot{E}_{\text{insolation}})[t]$ on the second row.

3.1. A Baseline Scenario

For clarity’s sake, we here neglect the influence of tides raised on the star (see §3.4), equivalent to setting $Q'_* \rightarrow \infty$. Figure 1 depicts the simultaneous evolution of the planet’s radius $R_p(t)$, eccentricity $e(t)$, semi-major axis $a(t)$, and power ratio $(\dot{E}_{\text{tide}}/\dot{E}_{\text{insolation}})[t]$ and demonstrates how tides raised on a close-in planet might induce a transient phase of radius inflation, with consequences on Gyr timescales. In this baseline case, $Q'_p = 10^{6.5}$ and $a_i = 0.075$ AU. We plot curves for different initial eccentricities ($e_i = 0.65, 0.60, 0.55, 0.40, 0.30, 0.20$) and in Fig. 1 use atmospheric opacities for solar-metallicity equilibrium chemical compositions. For comparison, we include two curves depicting cases with no tides and, therefore, no tidally-induced migration, zero eccentricity, but two different initial/final values of the semi-major axis (black dotted: $a = a_i = 0.075$ AU; black dashed: $a = 0.047$ AU, the current position of HD 209458b).

Typical behavior is illustrated by the curves on Fig. 1, for which $e_i = 0.65, 0.60, 0.55$. The very first episode of radius shrinkage is followed by a transient period of expansion, after which the radius resumes shrinking at a progressively slower rate. Let us describe the case for which $e_i = 0.65$. When $e_i = 0.65$, radius expansion starts at the age of ~ 0.13 Gyr ($R_p \simeq 1.48 R_J$), almost in phase with the increase in the power ratio ($\simeq 3 \times 10^{-3}$). The peak of the radius is reached at ~ 0.85 Gyr ($R_p \simeq 1.78 R_J$), and roughly coincides with the peak of the power ratio ($\simeq 8 \times 10^{-3}$), reached at ~ 0.80 Gyr. The corresponding time lag of ~ 50 Myr is not universal, but is generally shorter than the characteristic thermal cooling timescale. The latter depends more directly on diffusion through the thick atmosphere, while the former is more dependent on core tidal heating, to which the radius responds more directly. The average rate of radius expansion from the starting point of this phase to the peak is roughly $0.43 R_J \text{ Gyr}^{-1}$. The corresponding average rate of increase in the power ratio is $\sim 7 \text{ Gyr}^{-1}$. After the peak in the power ratio is achieved, it is followed by a drop at a rate of $\sim 4 \times 10^{-3} \text{ Gyr}^{-1}$. The rate at which R_p decreases is comparable to the rate at which it increases, until an age of ~ 1.2 Gyr, after which it progressively flattens and tends to zero, with an average value between 5 and 6 Gyr of $\sim 0.01 R_J \text{ Gyr}^{-1}$. It is important to reemphasize that all the variables R_p , e , a , and $\dot{E}_{\text{tide}}/\dot{E}_{\text{insolation}}$ are interdependent and evolve consistently by mutual influence. Thus, as suggested by eq. (6), the peak in the power ratio is the result of the combined evolution of e , a , and R_p , which in turn depends on this ratio. During the radius inflation phase, e and a decrease at a rate that increases in absolute value. The peak value of the planet’s radius corresponds closely to an inflection point in the evolution of e and a . After this inflection point, the absolute value of the rates of change of both e and a decrease, finally tending to zero.

While the circularizing orbit is gradually moving closer to the star, the stellar irradiation flux F_p is increasing and its role in stanching heat loss from the planet and slowing radius shrinkage is strengthened (Burrows et al. 2000). Once orbital equilibrium state has been achieved,

tidal effects disappear and R_p continues to evolve due to radiative losses from the surface (Burrows et al. 2007). Therefore, due to an earlier episode of tidal heating a planet’s orbit can currently be circular, and yet its radius can be larger than the default evolutionary theory would predict. In other words, a zero eccentricity orbit and, therefore, the absence of current tides, does not preclude an inflated radius due to the earlier action of tides. We will see in §3.4 that this equilibrium orbital state might not persist if we incorporate tides raised on the star and the corresponding Q'_* is small enough. Note that even if the maximum ratio $\dot{E}_{\text{tide}}/\dot{E}_{\text{insolation}}$ can appear quite small (e.g., $\sim 10^{-2}$), it can have a large effect on the orbital parameters and radius evolution (Liu et al. 2008).

For lower values of e_i , the duration of the transient phase increases, the maximum R_p achieved decreases, and the epoch of peak R_p shifts to older ages. The peak disappears altogether for values of e_i below between 0.40 and 0.30. However, this does not mean that tidal effects are no longer important. For lower values of e_i , tidal effects still slow the decrease in R_p . All else being equal, in particular for a given a_i , the lower the initial eccentricity e_i , the slower the evolution of the eccentricity to zero and the slower the evolution of the semi-major axis. In other words, the lower the value of e_i , the slower the evolution of both e and a and the higher the final a , for a given a_i . As for its impact on radius evolution, a lower e_i implies a weaker, but longer lasting, tidal influence. If e_i is small enough, the planet no longer receives enough tidal heat to inflate. All these outcomes are straightforwardly understood as consequences of eqs. (1), (2), (3), and (6), with $Q'_* \rightarrow \infty$. Thus, a lower value of e_i implies lower values of \dot{E}_{tide} and, therefore, less power to inflate the planet or reduce its rate of shrinkage. Clearly, it also implies a lower initial power ratio $\dot{E}_{\text{tide}}/\dot{E}_{\text{insolation}}$ and a slower rate of initial decrease of e and a . Furthermore, numerical integration of the set of evolutionary equations shows that this initial trend for e and a persists at later ages, even if the radii and power ratios “invert.” By this we mean that the radius at around 1 Gyr when $e_i = 0.65$, for example, can be much larger than the radius when $e_i = 0.20$. However, after ~ 3.5 Gyr it then decreases much faster and ends up smaller. Nevertheless, there is a small, but long lasting, tidal heating effect even in the case of $e_i = 0.20$. Eventually, the final radii are larger if the final semi-major axes are smaller, consistent with the conclusions of Burrows et al. (2007) – for a circular orbit, the closer the planet is to the star, the higher the insolation flux, and the larger its radius at a given epoch.

Comparing the case without tides, but with $a = a_i = 0.075$ AU (black dotted curve on Fig. 1), with those with non-zero values of e_i and the same a_i , demonstrates that the planet’s radius would always be larger when the planet can be tidally heated. However, even without tides the radius of a planet already at its current position (e.g., $a = 0.047$ AU, for HD 209458b) can be larger than the radius of a planet which experiences tidal heating. Fig. 1 demonstrates that, if the planet starts at a larger orbital distance, tidal heating does not necessarily and universally result in a larger planetary radius at a given age.

3.2. Extremely Strong Tidal Effects

As described in §3.1, tidal heating can have a significant, at times non-monotonic, impact on a close-in EGP’s radius evolution. This is a key conclusion. However, contrary to what one might naively expect, extremely strong tidal dissipation in a planet can have a negligible effect on its late-time radius. Figure 2 depicts the simultaneous evolution of a planet’s radius $R_p(t)$, eccentricity $e(t)$, semi-major axis $a(t)$, and power ratio $(\dot{E}_{\text{tide}}/\dot{E}_{\text{insolation}})[t]$ under such circumstances. For comparison, the same two tide-free cases depicted in Fig. 1 are also plotted in Fig. 2. The only difference with what was discussed in §3.1 is that we assume $Q'_p = 10^{5.0}$, instead of $Q'_p = 10^{6.5}$. We still assume $a_i = 0.075$ AU and ignore stellar tides. Models with only three of the initial eccentricities from Figure 1 are shown ($e_i = 0.40, 0.30, 0.20$), sufficient to demonstrate our point. Note that the plots focus on an earlier interval (2 Gyr).

In this case, after only ~ 10 Myr, whatever the initial eccentricity, R_p inexorably shrinks and the associated curves are much closer. This is despite the fact that in the early stages of evolution the power ratio, for $e_i = 0.40$ for example, is two orders of magnitude higher than in the baseline scenario of §3.1 – 10^{-1} compared with 10^{-3} . However, Fig. 2 indicates that such large additional core power has had only a small effect on the radius of the planet at the typical ages of observed transiting EGPs, i.e. at a few Gyr. This is because the orbit circularizes very rapidly and the tidal power ratio disappears extremely quickly. The final semi-major axis is reached in less than ~ 0.1 Gyr and the eccentricity is damped in less than ~ 0.8 Gyr. If we look at ages earlier than ~ 1 Gyr (not shown), we do see a transient phase of radius inflation for the case $e_i = 0.40$. The peak occurs very early (~ 10 Myr), is of very short duration, and though the planet’s radius can reach $\sim 3 R_J$, this transient phase lasts less than ~ 20 Myr. The radii, when there are tides (e.g., for $e_i = 0.40, 0.30, 0.20$), are close to one another simply because the final positions are close.

However, we suggest that the rapid onset of significant heating, followed by the muting of a significant effect on R_p at later times, might be an artifact of our initial conditions – such a combination of low Q'_p , high e_i , and small a_i may not have been allowed to establish itself without a more gradual feedback on the evolution that we, curiously, witness as an impulsive response. Before e_i would have been allowed to get that high or before a_i would have been allowed to get that small, tidal effects if $Q'_p = 10^5$ would no doubt have come into play. This conclusion does, however, depend upon the processes, and their timescales, that result in high e_i and in our initial a_i . If early migration and eccentricity pumping can occur on very short timescales, an early, almost impulsive, tidal response is possible.

3.3. Coupling Enhanced Atmospheric Opacity with Tidal Heating

If one increases the atmospheric opacity, due either to an increased metallicity or to the possible effects of photolysis and/or non-equilibrium chemistry, the planet retains heat better and can maintain a larger radius longer. This effect was previously explored by Burrows et al. (2007), who concluded that an enhanced opacity delays

radius shrinkage and can lead to larger EGP radii at a given age. They did their study for fixed circular orbits and presented results for solar and $10\times$ solar atmospheric opacity. Liu et al. (2008) also examined this effect, but at solar, $3\times$ solar, and $10\times$ solar opacities and explored the potential effects of tidal heating (at fixed, non-zero eccentricity). However, both studies kept the semi-major axis fixed. Here, we investigate the effect of enhanced opacity, but include orbit evolution as in §3.1 and §3.2. For specificity, we focus on atmospheric opacities equivalent to those for chemical equilibrium abundances at solar and $3\times$ solar metallicity.

Figure 3 depicts the simultaneous evolution of the planet’s radius $R_p(t)$, eccentricity $e(t)$, semi-major axis $a(t)$, and power ratio $(\dot{E}_{\text{tide}}/\dot{E}_{\text{insolation}})[t]$ for both solar (solid) and $3\times$ solar (dashed) atmospheric opacity. We present our results for an illustrative subset of eccentricities ($e_i = 0.60, 0.55, 0.40$), ignore tides raised on the star, and use the same parameters, $Q'_p = 10^{6.5}$ and $a_i = 0.075$ AU, employed in §3.1. The black curves are reference models with no tides and $a = a_i = 0.075$ AU. The black, dashed curve for $3\times$ solar with no tidal effects recapitulates the results already obtained by Burrows et al. (2007). At the age of ~ 1 Gyr, the radius increase effect is 5%.

The case for $e_i = 0.60$ and with tidal effects is particularly illustrative². With larger atmospheric opacity, the peaks in the radius and power ratio during the transient phase increase in magnitude, narrow, and shift towards younger ages. Note that when tidal effects are included in the comparison of the consequences of enhanced opacity, the results are not simply monotonic. For $e_i = 0.60$, an enhanced opacity leads first to a larger radius for ages up to ~ 0.9 Gyr, then to a smaller radius for ages up to ~ 2.8 Gyr, after which the planetary radius is again larger. Importantly, the higher the atmospheric opacity, the faster the eccentricity evolves to zero and the faster the semi-major axis tends to its final value. This is a consequence of the larger values of R_p possible with enhanced opacity and the stiff dependence of \dot{E}_{tide} on R_p . Interestingly, the final value of a is the same as that reached for the lower atmospheric opacity. Why do we end up with the same final equilibrium circular orbit, as indicated in Fig. 3, whereas in §3.1 different values of e_i resulted in different final orbits? This behavior can be derived directly from eqs. (1), (2), (3), and (6). For a given planet/star pair and the same values of Q'_p , e_i , and a_i , the amount of orbital energy transferred to the planet’s interior is the same. The increase in the atmospheric opacity decreases the rate of heat loss and the planet’s radius remains larger, longer. But this increase does not involve any transfer of energy inside the planet’s interior. This is why for identical initial orbital energies, the final orbital energies and, therefore, the final semi-major axes are the same. Angular momentum conservation can also be invoked to help explain this result. Hence, when tidal effects subside, the final radius with enhanced atmospheric opacity is indeed larger than the one obtained with solar opacity, but the same orbital parameters, all else being equal. However, as Fig. 3 indi-

² As Fig. 3 demonstrates, the qualitative behavior for different values of e_i is the same.

cates, the transient increase in R_p when the atmospheric opacity is larger can be quite dramatic.

3.4. The Particular Role of Tides Raised on the Star

Now, we examine what might happen when we include tidal dissipation in the star and set Q'_* equal to various non-trivial values. Figure 4 depicts the simultaneous evolution of $R_p(t)$, $e(t)$, $a(t)$, and $(\dot{E}_{\text{tide}}/\dot{E}_{\text{insolation}})[t]$ for $Q'_p = 10^{6.5}$, $a_i = 0.075$ AU, and solar-metallicity opacities, but this time for three different values of Q'_* : 10^6 (dashed), $10^{5.5}$ (dotted), and ∞ (solid). We replot from Fig. 1 the three cases with no stellar tides, but with $e_i = 0.60, 0.55, 0.40$, $Q'_p = 10^{6.5}$, and $a = a_i = 0.075$ AU. The solid black curve is for the case with no tides at all and $a = a_i = 0.075$ AU.

Let us focus our discussion on the three cases with $e_i = 0.60$, but for different values of Q'_* . Including stellar tides, the lower the value of Q'_* , the higher, narrower, and earlier are the peaks of the radius and power ratio during the early transient phase. This behavior is similar to that encountered in §3.3 with enhanced opacity or in §3.1 with higher initial eccentricity. This time, however, it is caused by the additional terms involving Q'_* in eqs. (1) and (2). As seen in Fig. 4, e and a decrease faster, but at a combined rate such that the ratios, $e^2/a^{11/2}$ in $\dot{E}_{\text{tide}}/\dot{E}_{\text{insolation}}$ (eq. 6) and $e^2/a^{15/2}$ in \dot{E}_{tide} (eq. 3), are bigger than in the case without stellar tides. Therefore, more orbital energy is dissipated faster in the planet's interior. As noted in §3.1 and §3.3, the evolution is quite non-monotonic and nonlinear. Moreover, even when there is no pronounced peak, as for $e_i = 0.40$, though the evolution is smoother, the general trends and behavior are similar.

The case of $e_i = 0.60$ and $Q'_* = 10^{5.5}$ is particularly interesting. Figure 4 shows that even after the orbit has already circularized ($e = 0$), the semi-major axis, instead of stabilizing at a constant value, continues to decrease. In fact, the planet starts to spiral inward at an accelerating rate, is eventually tidally disrupted, and collides with the star. Equation (9) in §2 gives the analytical evolution of a after circularization, ignoring tidal disruption. For $Q'_* = 10^{5.5}$ and $e_i = 0.60$, we intentionally stopped the evolution at $a = 0.02$ AU, which is at roughly the Roche limit for this system: $\sim 2.5(\rho_*/\rho_p)^{1/3} R_*$, where ρ_* and ρ_p are the average densities of the star and the planet, respectively. While the planet is spiraling in, Fig. 4 shows that R_p starts to shoot up.

This late-time behavior after the semi-axis has achieved small values and the orbital eccentricity is \sim zero has been seen before by Rasio et al. (1996), Levrard et al. (2009), Jackson et al. (2009), and Miller et al. (2009). However, whether such a dramatic effect would obtain depends sensitively on the value of Q'_* (Fig. 4) and on whether tidal effects in the planet can synergistically force a to achieve such low values that tidal dissipation in the star, which does not depend upon the eccentricity, can take over on stellar evolutionary timescales. It would seem unlikely that the current sample of transiting and close-in EGPs are those for which we are just now catching a last glimpse before they are eaten by the star. The implication for the parent population of exoplanets would appear extreme. However, at this stage, we cannot eliminate the outside possibil-

ity that, for a subset of very close-in EGPs, stellar tides might be important on timescales short compared with their corresponding stellar ages.

4. APPLICATION TO HD 209458B

The previous sections were devoted to investigating the generic behavior of R_p and orbital parameters when tidal dissipation in either the planet or the star is at work. Our main result is the emergence for a range of values of e_i and a_i of a transient phase of radius inflation which temporarily interrupts radius shrinkage. This phenomenon might explain the larger-than-otherwise-expected planetary radii of an interesting subset of the close-in transiting EGP population, either as a vestige of an epoch of earlier tidal heating, resetting the evolutionary clock (Liu et al. 2008), or as a current episode of significant tidal heating. An objective is to find a set of realistic values of Q'_p , Q'_* , e_i , and a_i for which the currently measured values of R_p , e , and a can be simultaneously explained. Other factors, such as the atmospheric opacity, the possible presence of a dense core, and the effect of a large heavy-element burden in the planetary envelope, also come into play, and custom fits for each EGP are necessary.

In this section, as an example we perform such an exercise for HD 209458b. However, the general procedures and the generic features apply to all large-radius EGPs (e.g., TrES-4, WASP-12b, and WASP-6b) for which transient tidal effects such as we have found in this paper are promising solutions. The observational data we use for HD 209458b are given in Table 1. Figure 5 depicts solar-opacity model evolutions of HD 209458b's radius $R_p(t)$, eccentricity $e(t)$, semi-major axis $a(t)$, and power ratio $(\dot{E}_{\text{tide}}/\dot{E}_{\text{insolation}})[t]$. We superpose on Fig. 5 the measured values of R_p , e , and a , with their error boxes. Also included on Fig. 5, but only in the top left panel, are four curves as reference cases with no tides. The dotted curve is for $a = a_i = 0.085$ AU. The other three non-solid curves are for solar, 3×solar, and 10×solar atmospheric opacities and for $a = 0.047$ AU, the measured value of HD 209458b's semi-major axis.

To fit the observations of HD 209458b, we have explored the effects of varying Q'_p and Q'_* from 10^5 to 10^8 , a_i from 0.10 AU to 0.055 AU, and e_i from 0.80 to 0.20. As a red line on Fig. 5, we identify the model with the best-fitting parameter set, obtained by trial and error. The associated parameters are: $Q'_p = 10^{6.55}$, $Q'_* = 10^{7.0}$, $a_i = 0.085$ AU, and $e_i = 0.77$. To illustrate the extreme sensitivity to model parameters, we plot curves for e_i ranging from 0.79 to 0.72, in steps of 0.01. Thus, by invoking this set of initial and planetary parameters and evolving the coupled suite of equations for R_p , e , and a , we can simultaneously explain the measured radius, eccentricity, and semi-major axis of HD 209458b. In §3.1, we described the sensitivity of the evolution to e_i . Indeed, when e_i decreases, the transient peaks of the radius and power ratio widen, their height diminishes, and the epoch of transient heating shifts to older ages. The semi-major axis decreases more slowly and settles at higher values. With $Q'_* = 10^{7.0}$, the tides raised on the star are not strong enough to lead to inspiral of HD 209458b into its host star on a timescale less than 6 Gyr. However, for $Q'_* = 10^{7.0}$ there is still a slight de-

crease of the semi-major axis during the 14-Gyr duration of the simulations (not shown). This demonstrates that, for this choice of parameters, the orbit of HD 209458b is effectively stable. For comparison, we have verified that values of Q'_* of $10^{6.0}$ and $10^{5.5}$ lead to inspiral of HD 209458b. However, the fit to the measurements is not as good. This example demonstrates how sensitive the results are to the values of the chosen parameters. Clearly, stronger independent constraints on these tidal Q' s are desirable.

Since the paper of Burrows et al. (2007), Torres et al. (2008) have reappraised the age of HD 209458b, from $5.5^{+1.5}_{-1.5}$ to $3.1^{+0.8}_{-0.7}$ Gyr. As a consequence, as Fig. 5 shows, the curves for $3\times$ solar and $10\times$ solar, but without tidal heating, now intercept the error box. We can in principle find a better fit if we choose an opacity between 3 and $10\times$ solar, but still without invoking tidal effects. Having said that, the introduction of tidal effects enables us to fit HD 209458b's radius easily even with solar-opacity atmospheres. In addition, we can now in principle provide a reasonable explanation for its observed eccentricity (and/or upper limit) and semi-major axis. Moreover, if one needed to invoke high-metallicity (not just high-opacity) atmospheres to explain HD 209458b's radius and, thereby high-metallicity envelopes, a transient tidal phase with significant heating now allows even the shrinking effect of heavy elements in the envelope to be compensated for. This system is a good example of a planet whose orbit has almost circularized, but that still has an inflated radius. Hence, as we have suggested in this subsection and in §3.1, the radius of HD 209458b may be due to the former action of tides during an earlier epoch of non-circular evolution. This explanation might also be germane to the TrES-4, WASP-12b, and WASP-6b planets, as well as to other large-radius EGPs.

There exists an interesting, if counterintuitive, systematic behavior in models for the simultaneous evolution of a , e , and R_p . For a given final position (a , e), an initially higher e_i does not necessarily result in a larger radius. The radius evolution is a strongly non-linear function of the initial conditions and as Fig. 1 indicates, different e_i s result in different radius evolutionary curves that intersect. Comparing radii for models with different initial values of a_i and e_i requires one to specify the age of the planet. Among the 7 curves on Fig. 5 (for $e_i=0.72$ to 0.79), only those for $e_i = 0.77$ and $= 0.76$ lie within the a , e , age, and R_p error boxes. Moreover, and perhaps counterintuitively, at the age of HD 209458b the radius for $e_i=0.77$ is smaller than the radius for $e_i=0.76$.

Hence, a model with a higher initial eccentricity peaks at a higher tidal heating rate, but at earlier ages. At the later times at which models with lower initial eccentricity peak, they have higher heating rates than the former at that same time. In the same vein, for the same e_i , starting with lower a_i results in a higher tidal heating rate at earlier ages than the tidal heating rate that eventually obtains when starting with a larger a_i .

5. CONCLUSIONS AND DISCUSSION

In this paper, we have found that if an EGP after early migration and dynamical evolution is left in a tight orbit ($a_i \lesssim 0.2$ AU) with a modest to high eccentricity ($\gtrsim 0.2$), its subsequent evolution due to tidal dissipation can qualitatively alter our interpretation of its measured

radius. Using a formalism in which the planet's radius and orbit are consistently and simultaneously evolved, we have found that a transient phase of rapid tidal heating and radius expansion can help explain the large radii measured for some transiting EGPs even after this phase has subsided. This explanation is straightforward for HD 209458b, but it might also be a factor in the large radii observed for, for example, TrES-4 (Mandushev et al. 2007; Torres et al. 2008; Sozzetti et al. 2009), WASP-12b (Hebb et al. 2009), WASP-6b (Gillon et al. 2009a), and WASP-4b (Wilson et al. 2008; Gillon et al. 2009b; Winn et al. 2009).

We parameterized our models using a range of planet and star tidal dissipation factors, a range of initial values of the eccentricity and semi-major axis, and three realizations of the planet's atmospheric opacity. Our main conclusions are:

- A giant planet's radius can undergo a transient phase of inflation due to tides that temporarily interrupts its shrinkage and resets its evolutionary clock. The upshot is that, for suitable parameters (e.g., Q'_p and Q'_* of $10^{5.0}$ – $10^{7.0}$, a_i less than ~ 0.2 AU, and $e_i \gtrsim 0.2$), R_p is measurably larger than it otherwise would have been, even after tidal heating has subsided. We have demonstrated that a planet whose orbit has circularized can still have an inflated radius due to the former action of tides.
- Extremely strong tidal heating in a planet will fade early in its life. Under such circumstances, the effect on R_p will be negligible at the typical ages of the observed transiting planets.
- Higher atmospheric opacities can enhance and accelerate the transient phase of radius inflation and accelerate orbital evolution.
- The tides raised on the star also enhance and accelerate the transient phase of radius inflation. However, even after the orbit circularizes due to tidal dissipation in the planet, the orbit does not stabilize – for small enough values of Q'_* , the planet can plunge inward, and is then tidally disrupted and consumed by the star.
- Radius and orbit evolution are strongly non-linear and stiff functions of the parameters Q'_p , Q'_* , e_i , a_i , and atmospheric opacity. Custom fits to each planet/star system, rather than pre-calculated look-up tables, are to be preferred.
- The parameters $(Q'_p, Q'_*, e_i, a_i) = (10^{6.55}, 10^{7.0}, 0.77, 0.085 \text{ AU})$, with a solar atmospheric opacity, provide a satisfactory fit to the measured radius of HD 209458b, while also being consistent with its current orbit. In general, the higher the atmospheric opacity the less tidal heating needs to be invoked to fit its observed R_p .
- Given its new, younger age, the measured radius of HD 209458b can now also be fit without tides, but only if the atmospheric opacity is similar to those with equilibrium chemical abundances for metallicities greater than $\sim 3\times$ solar. However, unless the atmospheric abundances can be measured, it will be difficult to distinguish the different predictions, particularly given the current ambiguity in

Q' . Nevertheless, if there are independent (theoretical?) constraints on Q' , and/or precision measurements of the atmospheric spectra, one might be able to discriminate between the two different explanations (vestigial tidal effects and higher atmospheric opacity).

There are numerous caveats that should be borne in mind when considering our results:

1. Our atmospheric boundary conditions assume that day side and night side cooling are the same. Credible general circulation models (GCMs) (Goodman 2008; Showman et al. 2008b,a,c; Dobbs-Dixon & Lin 2008; Langton & Laughlin 2008; Cho et al. 2008; Menou & Rauscher 2008) might address this issue most usefully.
2. We have fixed the properties of the host star during our integrations. On timescales of a few Gyr, the evolution of the star might be relevant.
3. The tidal dissipation factors Q' are very poorly constrained and are free parameters of our models. A firmer theoretical handle on their values and dependences would be very useful (Ogilvie & Lin 2004; Wu 2005a,b; Goodman & Lackner 2008).
4. We have assumed that the planet's spin is synchronized (tidally-locked) and have ignored the spin angular momentum of both the planet and the star. This is generally a good approximation, but there may be exceptional cases.
5. We have assumed that the tidal heating power is deposited solely in the convective zone, in which it is rapidly mixed. If much of the heat is instead deposited in the radiative atmosphere, as might be expected if circularization is dominated by Hough modes (Ogilvie & Lin 2007), our results would need alteration.
6. We have neglected the obliquities of both the star and the planet.

7. We start our calculations after early disk evolution and dispersal, and assume that the anomalously large planets, for which we might invoke tidal effects, are left after these early phases with high eccentricities and small semi-major axes. These assumptions are at present almost wholly unconstrained. We may, however, be able to turn the question around and someday use the current observations to constrain an earlier episode of vigorous tidal heating.

We have demonstrated that, given the right parameters and initial conditions, early tidal heating can result in large EGP radii, even while leaving the planet's current orbital parameters at modest values for which tidal heating is not expected to be important. These vestigial effects of an earlier transient phase might echo into the present to help explain the anomalously large radii of a small, but interesting, subset of transiting extrasolar giant planets. Our formalism can easily be applied to other inflated transiting EGPs, such as TrES-4 (Mandushev et al. 2007; Torres et al. 2008; Sozzetti et al. 2009), WASP-12b (Hebb et al. 2009), WASP-6b (Gillon et al. 2009a), and WASP-4b (Wilson et al. 2008; Gillon et al. 2009b; Winn et al. 2009), and we plan to do so in the near future.

We thank Ivan Hubeny for help with boundary condition issues, and Brian Jackson for instructive insights into the tidal evolution equations. We also thank Dave Spiegel, Jeremy Goodman, Rosemary Mardling, and Roman Rafikov for helpful discussions and an anonymous referee for suggesting changes that materially improved the manuscript. This study was supported by NASA grant NNX07AG80G and under JPL/Spitzer Agreements 1328092, 1348668, and 1312647.

REFERENCES

- Bakos, G. Á., Noyes, R. W., Kovács, G., Latham, D. W., Sasselov, D. D., Torres, G., Fischer, D. A., Stefanik, R. P., Sato, B., Johnson, J. A., Pál, A., Marcy, G. W., Butler, R. P., Esquerdo, G. A., Stanek, K. Z., Lázár, J., Papp, I., Sári, P., & Sipócz, B. 2007, *ApJ*, 656, 552
- Baraffe, I., Alibert, Y., Chabrier, G., & Benz, W. 2006, *A&A*, 450, 1221
- Baraffe, I., Chabrier, G., & Barman, T. 2008, *A&A*, 482, 315
- Baraffe, I., Chabrier, G., Barman, T. S., Allard, F., & Hauschildt, P. H. 2003, *A&A*, 402, 701
- Baraffe, I., Chabrier, G., Barman, T. S., Selsis, F., Allard, F., & Hauschildt, P. H. 2005, *A&A*, 436, L47
- Baraffe, I., Selsis, F., Chabrier, G., Barman, T. S., Allard, F., Hauschildt, P. H., & Lammer, H. 2004, *A&A*, 419, L13
- Barnes, R., Jackson, B., Raymond, S. N., West, A. A., & Greenberg, R. 2009, *ApJ*, 695, 1006
- Bodenheimer, P., Laughlin, G., & Lin, D. N. C. 2003, *ApJ*, 592, 555
- Bodenheimer, P., Lin, D. N. C., & Mardling, R. A. 2001, *ApJ*, 548, 466
- Burrows, A., Guillot, T., Hubbard, W. B., Marley, M. S., Saumon, D., Lunine, J. I., & Sudarsky, D. 2000, *ApJ*, 534, L97
- Burrows, A., Hubbard, W. B., Saumon, D., & Lunine, J. I. 1993, *ApJ*, 406, 158
- Burrows, A., Hubeny, I., Budaj, J., & Hubbard, W. B. 2007, *ApJ*, 661, 502
- Burrows, A., Hubeny, I., Hubbard, W. B., Sudarsky, D., & Fortney, J. J. 2004, *ApJ*, 610, L53
- Burrows, A., Marley, M., Hubbard, W. B., Lunine, J. I., Guillot, T., Saumon, D., Freedman, R., Sudarsky, D., & Sharp, C. 1997, *ApJ*, 491, 856
- Burrows, A., Sudarsky, D., & Hubbard, W. B. 2003, *ApJ*, 594, 545
- Chabrier, G. & Baraffe, I. 2007, *ApJ*, 661, L81
- Chabrier, G., Barman, T., Baraffe, I., Allard, F., & Hauschildt, P. H. 2004, *ApJ*, 603, L53
- Charbonneau, D., Brown, T. M., Latham, D. W., & Mayor, M. 2000, *ApJ*, 529, L45
- Chatterjee, S., Ford, E. B., Matsumura, S., & Rasio, F. A. 2008, *ApJ*, 686, 580
- Cho, J. Y.-K., Menou, K., Hansen, B. M. S., & Seager, S. 2008, *ApJ*, 675, 817
- Darwin, G. H. 1880, *Nature*, 21, 235

- Dickey, J. O., Bender, P. L., Faller, J. E., Newhall, X. X., Ricklefs, R. L., Ries, J. G., Shelus, P. J., Veillet, C., Whipple, A. L., Wiant, J. R., Williams, J. G., & Yoder, C. F. 1994, *Science*, 265, 482
- Dobbs-Dixon, I. & Lin, D. N. C. 2008, *ApJ*, 673, 513
- Dobbs-Dixon, I., Lin, D. N. C., & Mardling, R. A. 2004, *ApJ*, 610, 464
- Eggleton, P. P., Kiseleva, L. G., & Hut, P. 1998, *ApJ*, 499, 853
- Fabrycky, D. C., Johnson, E. T., & Goodman, J. 2007, *ApJ*, 665, 754
- Ferraz-Mello, S., Rodríguez, A., & Hussmann, H. 2008, *Celestial Mechanics and Dynamical Astronomy*, 101, 171
- Ford, E. B. & Rasio, F. A. 2008, *ApJ*, 686, 621
- Ford, E. B., Rasio, F. A., & Yu, K. 2003, in *Astronomical Society of the Pacific Conference Series*, Vol. 294, *Scientific Frontiers in Research on Extrasolar Planets*, ed. D. Deming & S. Seager, 181–188
- Fortney, J. J. & Hubbard, W. B. 2004, *ApJ*, 608, 1039
- Fortney, J. J., Marley, M. S., & Barnes, J. W. 2007, *ApJ*, 659, 1661
- Fortney, J. J., Marley, M. S., Saumon, D., & Lodders, K. 2008, *ApJ*, 683, 1104
- Gavrilov, S. V. & Zharkov, V. N. 1977, *Icarus*, 32, 443
- Gillon, M., Anderson, D. R., Triaud, A. H. M. J., Hellier, C., Maxted, P. F. L., Pollaco, D., Queloz, D., Smalley, B., West, R. G., Wilson, D. M., Bentley, S. J., Collier Cameron, A., Enoch, B., Hebb, L., Horne, K., Irwin, J., Joshi, Y. C., Lister, T. A., Mayor, M., Pepe, F., Parley, N., Segransan, D., Udry, S., & Wheatley, P. J. 2009a, submitted to *A&A* (arXiv:0901.4705)
- Gillon, M., Smalley, B., Hebb, L., Anderson, D. R., Triaud, A. H. M. J., Hellier, C., Maxted, P. F. L., Queloz, D., & Wilson, D. M. 2009b, *A&A*, 496, 259
- Goldreich, P. & Sari, R. 2003, *ApJ*, 585, 1024
- Goldreich, P. & Soter, S. 1966, *Icarus*, 5, 375
- Goldreich, R. 1963, *MNRAS*, 126, 257
- Goodman, J. 2008, (arXiv:0810.1282)
- Goodman, J. & Lackner, C. 2008, submitted to *ApJ* (arXiv:0812.1028)
- Gu, P.-G., Bodenheimer, P. H., & Lin, D. N. C. 2004, *ApJ*, 608, 1076
- Gu, P.-G., Lin, D. N. C., & Bodenheimer, P. H. 2003, *ApJ*, 588, 509
- Guillot, T., Burrows, A., Hubbard, W. B., Lunine, J. I., & Saumon, D. 1996, *ApJ*, 459, L35+
- Guillot, T., Santos, N. C., Pont, F., Iro, N., Melo, C., & Ribas, I. 2006, *A&A*, 453, L21
- Guillot, T. & Showman, A. P. 2002, *A&A*, 385, 156
- Hebb, L., Collier-Cameron, A., Loeillet, B., Pollacco, D., Hébrard, G., Street, R. A., Bouchy, F., Stempels, H. C., Moutou, C., Simpson, E., Udry, S., Joshi, Y. C., West, R. G., Skillen, I., Wilson, D. M., McDonald, I., Gibson, N. P., Aigrain, S., Anderson, D. R., Benn, C. R., Christian, D. J., Enoch, B., Haswell, C. A., Hellier, C., Horne, K., Irwin, J., Lister, T. A., Maxted, P., Mayor, M., Norton, A. J., Parley, N., Pont, F., Queloz, D., Smalley, B., & Wheatley, P. J. 2009, *ApJ*, 693, 1920
- Hubeny, I. & Lanz, T. 1995, *ApJ*, 439, 875
- Hut, P. 1981, *A&A*, 99, 126
- Jackson, B., Barnes, R., & Greenberg, R. 2008a, *MNRAS*, 391, 237
- Jackson, B., Greenberg, R., & Barnes, R. 2008b, in *IAU Symposium*, Vol. 249, *IAU Symposium*, 187–196
- Jackson, B., Greenberg, R., & Barnes, R. 2008c, *ApJ*, 678, 1396
- , 2008d, *ApJ*, 681, 1631
- Jackson, B., Greenberg, R., & Barnes, R. 2009, in *American Astronomical Society Meeting Abstracts*, Vol. 213, *American Astronomical Society Meeting Abstracts*, 351.01
- Johns-Krull, C. M., McCullough, P. R., Burke, C. J., Valenti, J. A., Janes, K. A., Heasley, J. N., Prato, L., Bissinger, R., Fleenor, M., Foote, C. N., Garcia-Melendo, E., Gary, B. L., Howell, P. J., Mallia, F., Masi, G., & Vanmunster, T. 2008, *ApJ*, 677, 657
- Johnson, J. A., Winn, J. N., Narita, N., Enya, K., Williams, P. K. G., Marcy, G. W., Sato, B., Ohta, Y., Taruya, A., Suto, Y., Turner, E. L., Bakos, G., Butler, R. P., Vogt, S. S., Aoki, W., Tamura, M., Yamada, T., Yoshii, Y., & Hidas, M. 2008, *ApJ*, 686, 649
- Jurić, M. & Tremaine, S. 2008, *ApJ*, 686, 603
- Kaula, W. M. 1968, *An introduction to planetary physics - The terrestrial planets* (Space Science Text Series, New York: Wiley, 1968)
- Knutson, H. A., Charbonneau, D., Noyes, R. W., Brown, T. M., & Gilliland, R. L. 2007, *ApJ*, 655, 564
- Kurucz, R. 1994, *Solar abundance model atmospheres for 0,1,2,4,8 km/s*. Kurucz CD-ROM No. 19. Cambridge, Mass.: Smithsonian Astrophysical Observatory, 1994., 19
- Langton, J. & Laughlin, G. 2008, *ApJ*, 674, 1106
- Laughlin, G., Wolf, A., Vanmunster, T., Bodenheimer, P., Fischer, D., Marcy, G., Butler, P., & Vogt, S. 2005, *ApJ*, 621, 1072
- Levrard, B., Correia, A. C. M., Chabrier, G., Baraffe, I., Selsis, F., & Laskar, J. 2007, *A&A*, 462, L5
- Levrard, B., Winisdoerffer, C., & Chabrier, G. 2009, *ApJ*, 692, L9
- Liu, X., Burrows, A., & Ibgui, L. 2008, *ApJ*, 687, 1191
- Love, A. E. H. 1927, *A Treatise on the Mathematical Theory of Elasticity* (Dover, New York)
- Madhusudhan, N. & Winn, J. N. 2009, *ApJ*, 693, 784
- Mandushev, G., O'Donovan, F. T., Charbonneau, D., Torres, G., Latham, D. W., Bakos, G. Á., Dunham, E. W., Sozzetti, A., Fernández, J. M., Esquerdo, G. A., Everett, M. E., Brown, T. M., Rabus, M., Belmonte, J. A., & Hillenbrand, L. A. 2007, *ApJ*, 667, L195
- Mardling, R. A. 2007, *MNRAS*, 382, 1768
- Mardling, R. A. & Lin, D. N. C. 2002, *ApJ*, 573, 829
- , 2004, *ApJ*, 614, 955
- Marley, M. S., Fortney, J. J., Hubickyj, O., Bodenheimer, P., & Lissauer, J. J. 2007, *ApJ*, 655, 541
- Menou, K. & Rauscher, E. 2008, submitted to *ApJ* (arXiv:0809.1671)
- Miller, N., Fortney, J., & Jackson, B. 2009, *B.A.A.S.* 402.07
- Murray, C. D. & Dermott, S. F. 1999, *Solar system dynamics* (Solar system dynamics by Murray, C. D., 1999)
- Nagasawa, M., Ida, S., & Bessho, T. 2008, *ApJ*, 678, 498
- Ogilvie, G. I. & Lin, D. N. C. 2004, *ApJ*, 610, 477
- , 2007, *ApJ*, 661, 1180
- Peale, S. J. & Cassen, P. 1978, *Icarus*, 36, 245
- Rasio, F. A., Tout, C. A., Lubow, S. H., & Livio, M. 1996, *ApJ*, 470, 1187
- Saumon, D., Chabrier, G., & van Horn, H. M. 1995, *ApJS*, 99, 713
- Showman, A. P., Cooper, C. S., Fortney, J. J., & Marley, M. S. 2008a, *ApJ*, 682, 559
- Showman, A. P., Fortney, J. J., Lian, Y., Marley, M. S., Freedman, R. S., Knutson, H. A., & Charbonneau, D. 2008b, submitted to *ApJ* (arXiv:0809.2089)
- Showman, A. P. & Guillot, T. 2002, *A&A*, 385, 166
- Showman, A. P., Menou, K., & Cho, J. Y.-K. 2008c, in *Astronomical Society of the Pacific Conference Series*, Vol. 398, *Astronomical Society of the Pacific Conference Series*, ed. D. Fischer, F. A. Rasio, S. E. Thorsett, & A. Wolszczan, 419–+
- Sozzetti, A., Torres, G., Charbonneau, D., Winn, J. N., Korzennik, S. G., Holman, M. J., Latham, D. W., Laird, J. B., Fernandez, J., O'Donovan, F. T., Mandushev, G., Dunham, E., Everett, M. E., Esquerdo, G. A., Rabus, M., Belmonte, J. A., Deeg, H. J., Brown, T. N., Hidas, M. G., & Baliber, N. 2009, *ApJ*, 691, 1145
- Torres, G., Winn, J. N., & Holman, M. J. 2008, *ApJ*, 677, 1324
- Wilson, D. M., Gillon, M., Hellier, C., Maxted, P. F. L., Pepe, F., Queloz, D., Anderson, D. R., Collier Cameron, A., Smalley, B., Lister, T. A., Bentley, S. J., Blecha, A., Christian, D. J., Enoch, B., Haswell, C. A., Hebb, L., Horne, K., Irwin, J., Joshi, Y. C., Kane, S. R., Marmier, M., Mayor, M., Parley, N., Pollacco, D., Pont, F., Rians, R., Segransan, D., Skillen, I., Street, R. A., Udry, S., West, R. G., & Wheatley, P. J. 2008, *ApJ*, 675, L113
- Winn, J. N. & Holman, M. J. 2005, *ApJ*, 628, L159
- Winn, J. N., Holman, M. J., Bakos, G. Á., Pál, A., Johnson, J. A., Williams, P. K. G., Shporer, A., Mazeh, T., Fernandez, J., Latham, D. W., & Gillon, M. 2007, *AJ*, 134, 1707
- Winn, J. N., Holman, M. J., Carter, J. A., Torres, G., Osip, D. J., & Beatty, T. 2009, *AJ*, 137, 3826
- Winn, J. N., Holman, M. J., Torres, G., McCullough, P., Johns-Krull, C., Latham, D. W., Shporer, A., Mazeh, T., Garcia-Melendo, E., Foote, C., Esquerdo, G., & Everett, M. 2008, *ApJ*, 683, 1076

Wu, Y. 2003, in *Astronomical Society of the Pacific Conference Series*, Vol. 294, *Scientific Frontiers in Research on Extrasolar Planets*, ed. D. Deming & S. Seager, 213–216
Wu, Y. 2005a, *ApJ*, 635, 674
—. 2005b, *ApJ*, 635, 688

Wu, Y. & Murray, N. 2003, *ApJ*, 589, 605
Wu, Y., Murray, N. W., & Ramsahai, J. M. 2007, *ApJ*, 670, 820
Yoder, C. F. & Peale, S. J. 1981, *Icarus*, 47, 1

TABLE 1
OBSERVATIONAL DATA OF THE HD 209458 SYSTEM.

Planet	a (AU)	e (95.4% confidence)	period (days)	M_p (M_J)	R_p (R_J)
HD 209458b	$0.04707^{+0.00046}_{-0.00047}$	< 0.028	3.524746	$0.685^{+0.015}_{-0.014}$	$1.320^{+0.024}_{-0.025}$

Star	M_* M_\odot	R_* R_\odot	T_* (K)	$[Fe/H]_*$ (dex)	age (Gyr)
HD 209458	$1.101^{+0.066}_{-0.062}$	$1.125^{+0.020}_{-0.023}$	6065^{+50}_{-50}	$0.00^{+0.05}_{-0.05}$	$3.1^{+0.8}_{-0.7}$

NOTE. — Data are from Knutson et al. (2007), Torres et al. (2008), and Madhusudhan & Winn (2009).

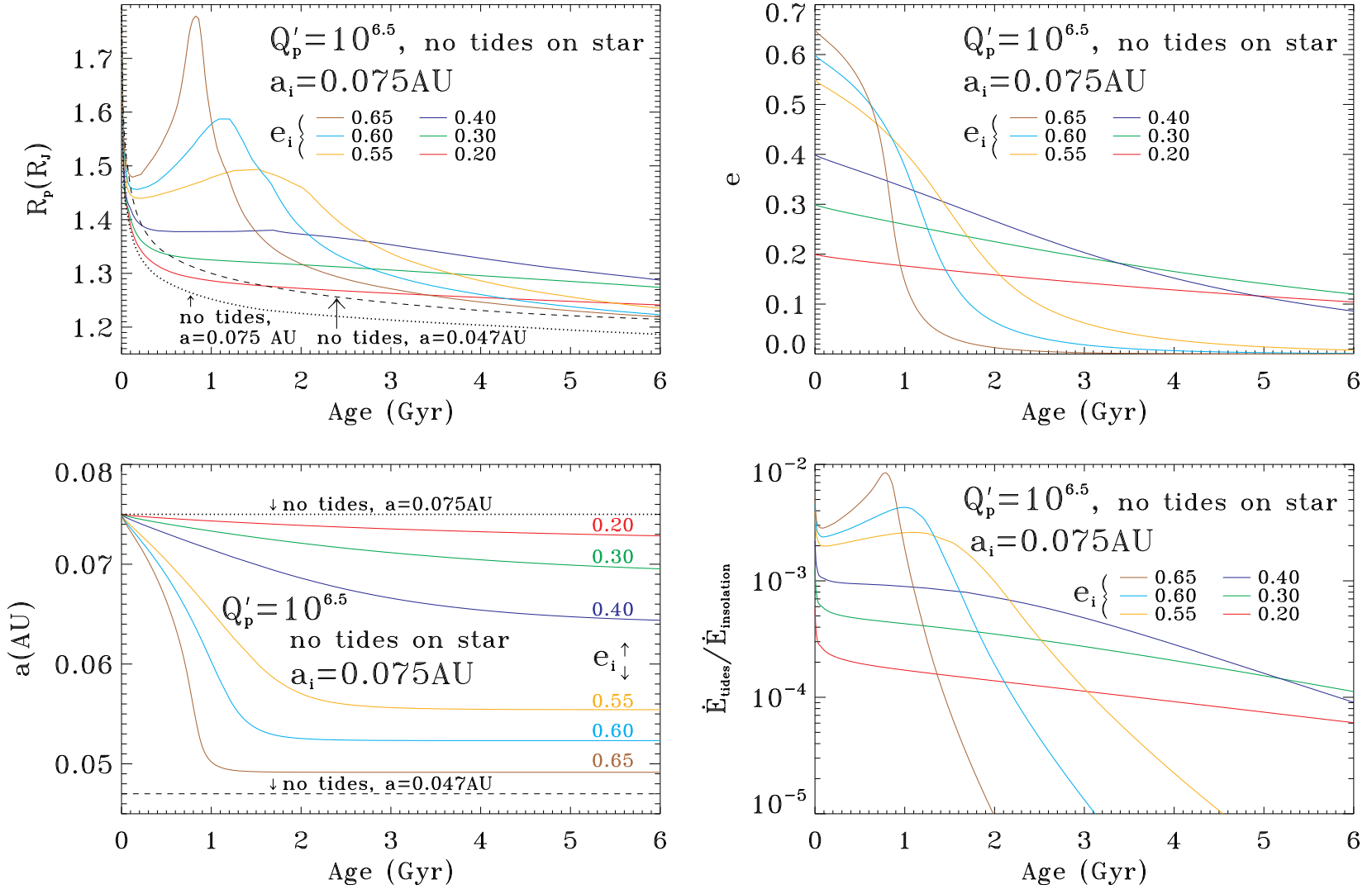


FIG. 1.— The Baseline scenario. Shown are the evolution of the planet radius R_p (R_J) (top left), eccentricity e (top right), semi-major axis a (AU) (bottom left), and power ratio $\dot{E}_{\text{tides}}/\dot{E}_{\text{insolation}}$ (bottom right) versus age (in Gyr) for a representative planet (taken to be HD 209458b) at solar atmospheric opacity. Q'_p is set equal to $10^{6.5}$ and a_i is set equal to 0.075 AU. We neglect tides raised on the star ($Q'_* \rightarrow \infty$). e_i assumes values of 0.2, 0.3, 0.4, 0.55, 0.60, and 0.65 (different colors). Also shown in the left panels are radius evolution curves with no tides – $a = a_i$ (dotted) and $a = a_{\text{measured}} = 0.047$ AU (dashed). For $e_i = (0.65, 0.60, 0.55)$, the evolution undergoes a transient phase of radius inflation. This phase does not appear for lower values of e_i (0.40, 0.30, 0.20), but the radius increase effect at later times is still in evidence. The orbits eventually achieve circular equilibrium states – the higher the e_i , the closer to the star. See the discussion in §3.1.

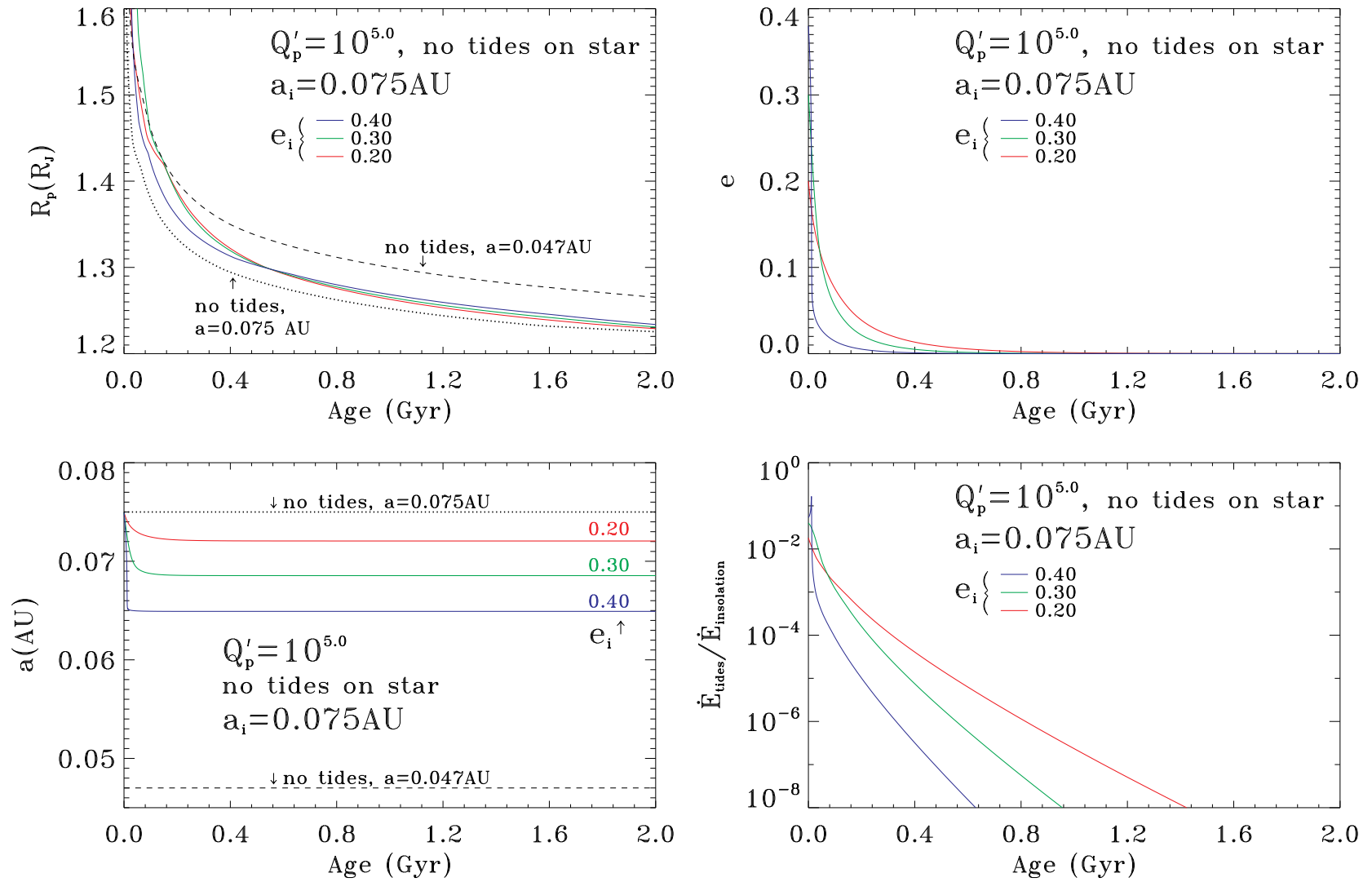


FIG. 2.— The same as in Fig. 1, but for the case of very strong planetary tidal effects (at a low value of $Q'_p = 10^5$) and for the first 2 Gyr. Also shown on the two left panels are two reference radius evolution curves incorporating no tides – one for $a = a_i$ (dotted) and one for $a = a_{\text{measured}} = 0.047$ AU (dashed). Models for only a subset of values of e_i (0.20, 0.30, 0.40) are depicted. The tidal effects fade at very early stages, so that their effect on radius evolution is quite small at the observed ages of transiting planets, a few Gyr. The orbits circularize in less than ~ 0.8 Gyr. See the text in §3.2 for a discussion.

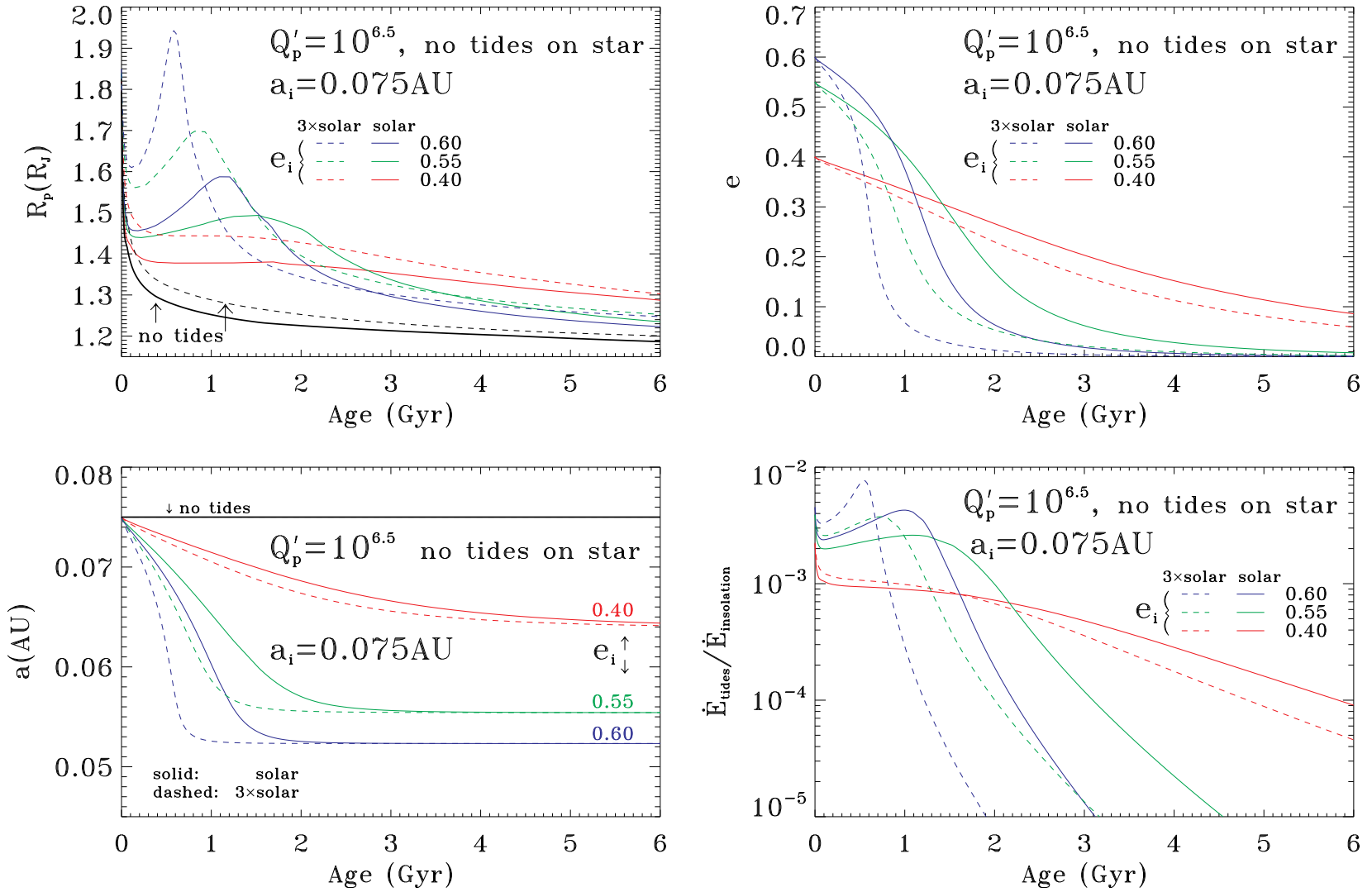


FIG. 3.— Same as in Fig. 1, but depicting the effect of atmospheric opacity. Models for opacities with equilibrium chemical abundances at solar (solid) and 3×solar (dashed) metallicity are compared. The initial eccentricities e_i are 0.40, 0.55, and 0.60 and they are distinguished by different colors. The planetary tidal dissipation factor (Q'_p) is set equal to $10^{6.5}$ and the tides raised on the star are neglected ($Q'_* \rightarrow \infty$). a_i is set equal to 0.075 AU. Also shown on the top left panel are two radius evolution curves with no tides – for $a = a_i$ at solar (solid) and 3×solar (dashed) equilibrium opacities. The final orbital state for the two opacities is the same, but that with higher opacity reaches it earlier. See the text in §3.3 for a more complete discussion.

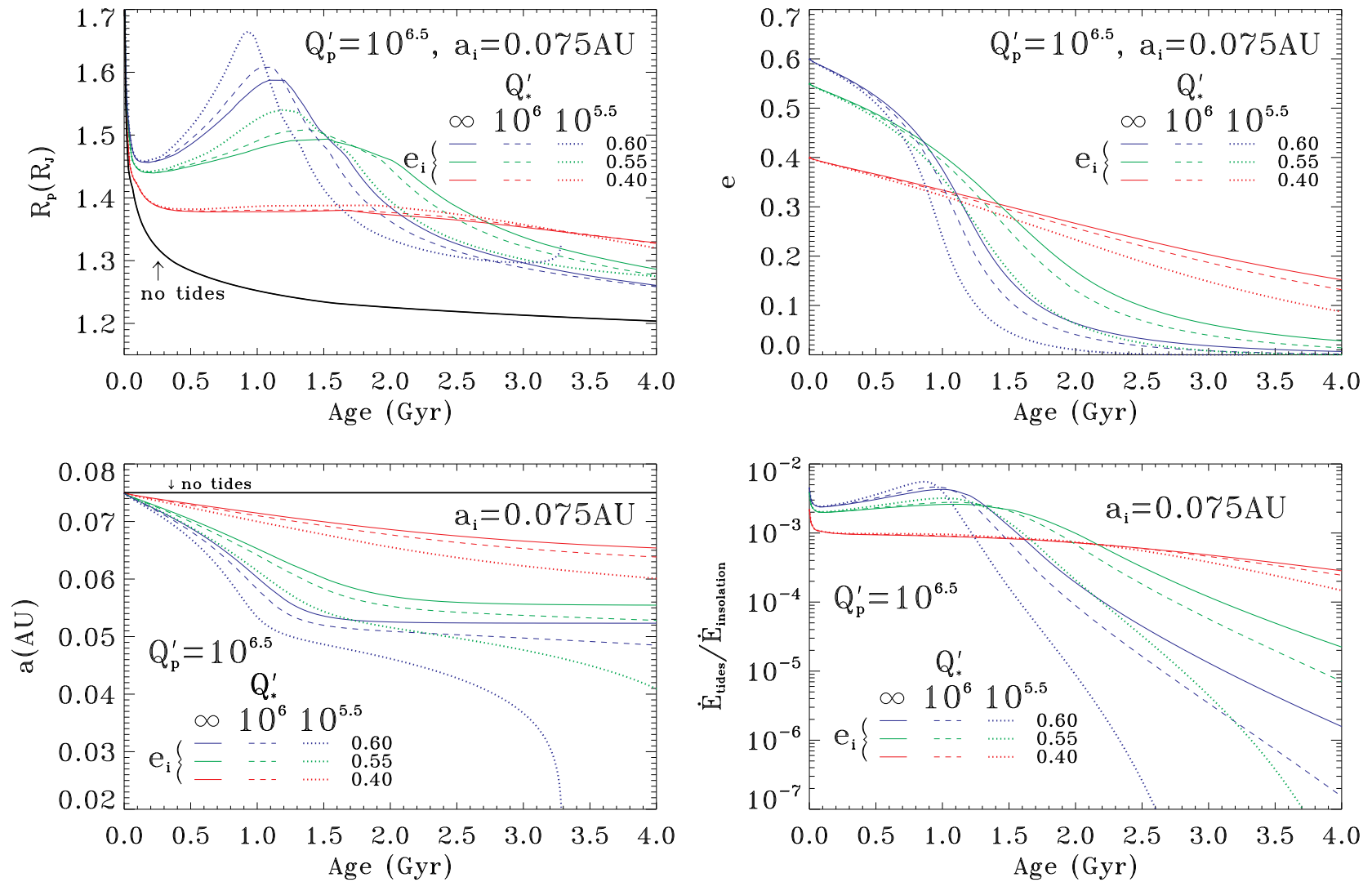


FIG. 4.— Same as Fig. 1, but portraying the effect of tides raised on the star. Models for values of Q'_* of ∞ (solid), $10^{6.0}$ (dashed), and $10^{5.5}$ (dotted) are compared. e_i is set equal to 0.40, 0.50, and 0.60 and these models are distinguished by different colors. $a_i = 0.075$ AU for all models and Q'_p is the same for all models ($10^{6.5}$). Also shown for reference in the two left panels is a model without tidal effects at all for $a = a_i$. Lower values of Q'_* enhance and accelerate the transient phase of radius inflation. The orbits generally evolve faster, eventually circularize, but do not reach an equilibrium state. The evolution of a for $Q'_* = 10^{5.5}$ and $e_i = 0.60$ (purple dotted curve) indicates that a planet with such parameters eventually spirals into the star after ~ 3.3 Gyrs (at an accelerating pace at later times). See the text in §3.4 for a discussion.

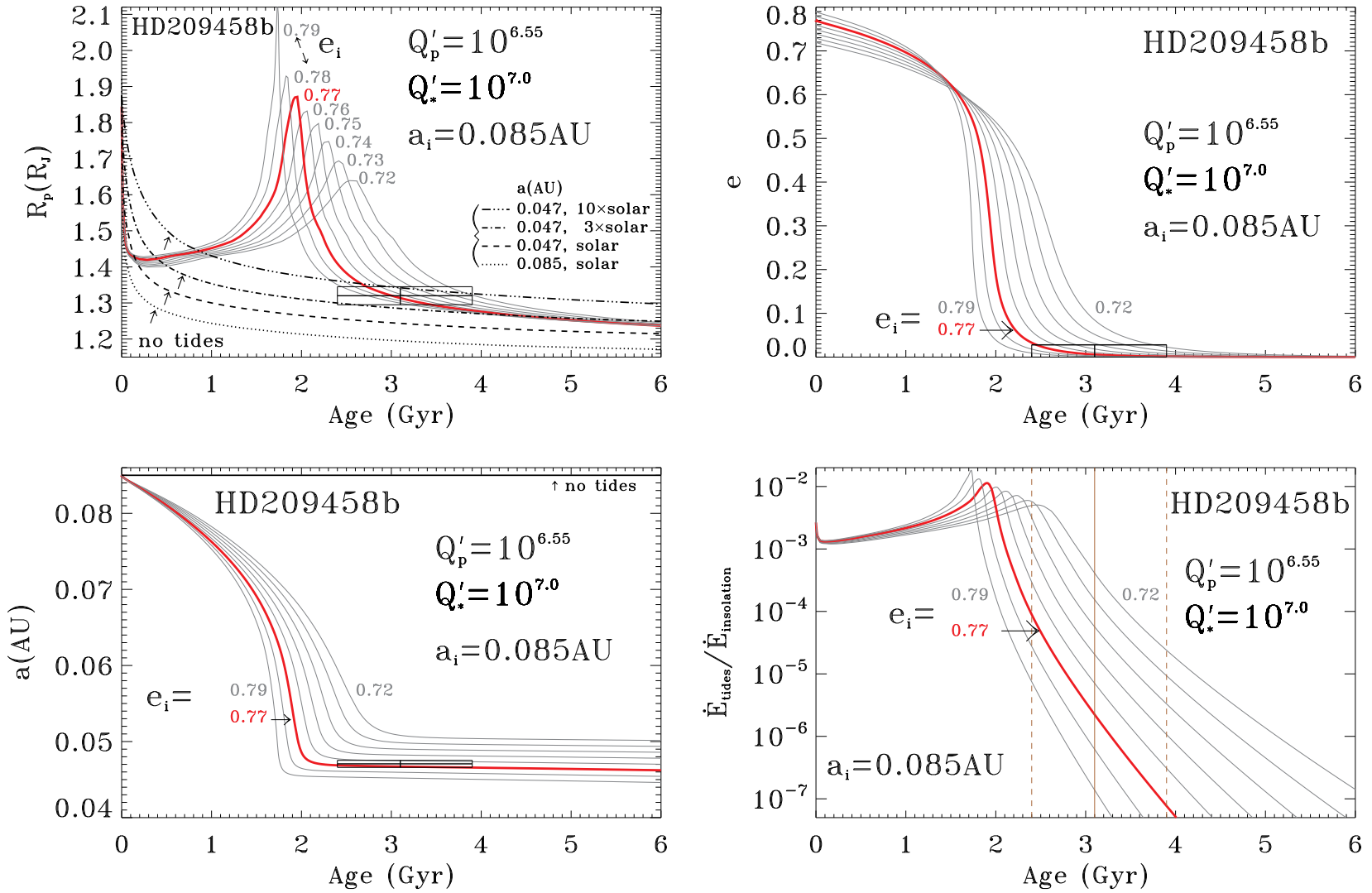


FIG. 5.— Example fit of the observed values of R_p , e , and a for HD 209458b. The measured R_p , e , and a are shown with error boxes. The best fitting curve is for $e_i = 0.77$, $Q'_p = 10^{6.55}$, and $Q'_* = 10^{7.0}$. This model is shown in red. We have used $a_i = 0.085$ AU. To demonstrate the strong dependence on e_i , we include models for e_i between 0.72 and 0.79. Also shown in the top left panel are four radius evolution curves (in non-solid black) that ignore the effects of tides. They are for $a = a_i$, but also for $a = a_{\text{measured}} = 0.047$ AU at solar, 3×solar, and 10×solar atmospheric opacities. The best fitting curves without tidal effects are for $\gtrsim 3$ ×solar. See the text in §4 for a discussion.